Contribution of Rock Glacier Discharge to Late-Summer and Fall Streamflow in the Uinta Mountains, Utah, USA

Jeffrey S. Munroe[1], Alexander L. Handwerger[2,3]

[1] Department of Earth & Climate Sciences, Middlebury College, Middlebury, 05753, USA

[2] Joint Institute for Regional Earth System Science and Engineering, University of California, Los Angeles, 90095, USA

[3] Jet Propulsion Laboratory, California Institute of Technology, Pasadena, 91109, USA

Correspondence to: Jeffrey S. Munroe (jmunroe@middlebury.edu)

Abstract. Water draining from rock glaciers in the Uinta Mountains of Utah (USA) was analyzed and compared with samples of groundwater and water from the master stream in a representative 5000-ha drainage. Rock glacier water resembles snowmelt in the early summer, but evolves to higher values of *d-excess* and greatly elevated Ca and Mg content as the melt season progresses. This pattern is consistent with models describing a transition from snowmelt, to melting of seasonal ice, to melting of perennial ice in the rock glacier interior in late summer and fall. Water derived from this internal ice appears to have been the source of ~25% of the streamflow in this study area during September of 2021. This result emphasizes the significant role that rock glaciers can play in the hydrology of high-elevation watersheds, particularly in summers following a winter with below average snowpack.

Keywords: Rock glacier; hydrology; permafrost; stable isotopes; climate change

1 Introduction

Contemporary climate change is responsible for an array of dramatic effects in high mountain environments (Adler et al., 2019; Chakraborty, 2021). Average temperatures of air (Bonfils et al., 2008; Minder et al., 2018) and permafrost (Biskaborn et al., 2019) are rising, glaciers are retreating (Sakai and Fujita, 2017; Sommer et al., 2020), the ranges of plants (Alexander et al., 2018; Albrich et al., 2020) and animals (Millar and Westfall, 2010; Rödder et al., 2021) are shifting, and ecosystem services (Egan and Price, 2017; Palomo, 2017) and the societies that depend on them (McDowell et al., 2019; Xenarios et al., 2019) are in a phase of readjustment. Documenting and understanding these changes is of crucial importance in mitigating natural hazards (Stoffel and Corona, 2018; Thaler et al., 2018), anticipating future scarcity of water resources (Beniston et al., 2018; Rowan et al., 2018), designing appropriate conservation strategies (Catalan et al., 2017), and planning for a future in which mountain environments look and function differently than they have for the past century (Huss et al., 2017).

33   A component of mountain landscapes with strong potential to document past and present environmental
34 changes, and a notable vulnerability to climatic perturbations, are features known as rock glaciers. Typically present
35 in cold environments that are too dry for the formation of ice glaciers, rock glaciers are mixtures of rock debris and
36 perennial ice that move downslope through a combination of creep and basal shear (Wahrhaftig and Cox, 1959;
37 Giardino et al., 1987; Giardino and Vitek, 1988). Given their genesis, their composition, and their behavior, rock
38 glaciers exist at the intersection of climate, the cryosphere, and hydrology.

39   Traditionally, rock glacier research focused on the distribution and paleoclimatic significance of these
40 features (Konrad et al., 1999; Johnson et al., 2021). Modern updates to these investigations are applying high
41 precision GPS (Buchli et al., 2018), photogrammetry (Kenner et al., 2018), surface-exposure dating (Lehmann et al.,
42 2022), and remote sensing to monitor rock glacier movement (Strozzi et al., 2020), offering an unprecedented
43 understanding of the relationship between rock glacier behavior and climate change. Studies have also sought to
44 explore the role of rock glaciers as refugia for cold-adapted organisms in the face of warming temperatures (Millar
45 et al., 2015; Brighenti et al., 2021).

46   An additional topic with critical importance in regions characterized by water scarcity is the contribution of
47 rock glaciers to high mountain hydrology (Rangecroft et al., 2015; Jones et al., 2019). The interconnected pore
48 space within the typically coarse debris comprising a rock glacier allows these features to serve as aquifers, storing
49 and releasing water over a variety of timescales (Geiger et al., 2014; Harrington et al., 2018; Wagner et al., 2020;
50 Halla et al., 2021). Moreover, perennial ice within the interior of an active rock glacier is a reservoir of longer-term
51 storage that is nonetheless vulnerable to being lost from the system through melting in excess of new ice formation.
52 Studies have investigated the ice content of rock glaciers using geophysical methods such as ground penetrating
53 radar and invasive approaches like drilling (Krainer and Mostler, 2002; Krainer et al., 2015; Petersen et al., 2020;
54 Wagner et al., 2021). Extrapolation from these investigations, and incorporation of empirical transfer functions, has
55 supported estimates of rock glacier water storage for some areas (Azócar and Brenning, 2010; Rangecroft et al.,
56 2015; Janke et al., 2017; Jones et al., 2018). Nonetheless, uncertainty remains about how much ice is stored within
57 rock glaciers, the vulnerability of this ice to climate warming, and how much ice may already be melting and
58 contributing to base flow, particularly in late summer after the melting of seasonal snow has ceased.

59   Here we investigate the water draining from representative rock glaciers in the Uinta Mountains in
60 northeastern Utah, a mountain range in which rock glaciers have been inventoried (Munroe, 2018) and monitored
61 (Brencher et al., 2021) in previous work. Automated samplers were used to collect time series of water discharging
62 from two rock glaciers, a non-rock glacier spring, and along the master stream. All samples were analyzed for
63 cation chemistry and stable isotopes to test two related hypotheses: 1) that the rock glacier springs would exhibit
64 properties distinct from the other water sources and consistent with the melting of internal ice in late summer; and 2)
65 that late summer streamflow along the master stream would contain a non-trivial amount of rock glacier-sourced
66 water.

67

2 Study Area

The study area for this project is in the upper West Fork Whiterocks River watershed in the southeastern sector of the Uinta Mountains (Figure 1). The watershed has an area of ~5000 ha above the lowest sampling site, and elevations range from 2960 to over 3700 m. The Uinta Mountains (hereafter, the "Uintas") are a substantial component of the Rocky Mountain system located in northeastern Utah in the western United States. The Uintas are the highest mountains in this region, reaching elevations in excess of 4 km. The bedrock of the Uintas is a thick sequence of Precambrian siliciclastic rocks that was uplifted during the Laramide orogeny beginning in the early Paleogene (Sears et al., 1982; Hansen, 1986; Dehler et al., 2007). Pleistocene valley glaciers eroded deep cirques and glacial canyons, and deposited massive lateral and end moraine systems (Atwood, 1909; Munroe and Laabs, 2009). No ice glaciers remain in these mountains today, however the climate at higher elevations, where mean annual temperatures are <0 °C (Munroe, 2006), supports patterned ground, talus, and abundant rock glaciers. Previous work using optical imagery (Munroe, 2018) and satellite-based radar interferometry (Brencher et al., 2021) identified more than 200 active rock glaciers in the Uintas, and many more that are no longer moving. Eight rock glaciers totaling 170 ha are mapped within the West Fork Whiterocks drainage (Figure 1).
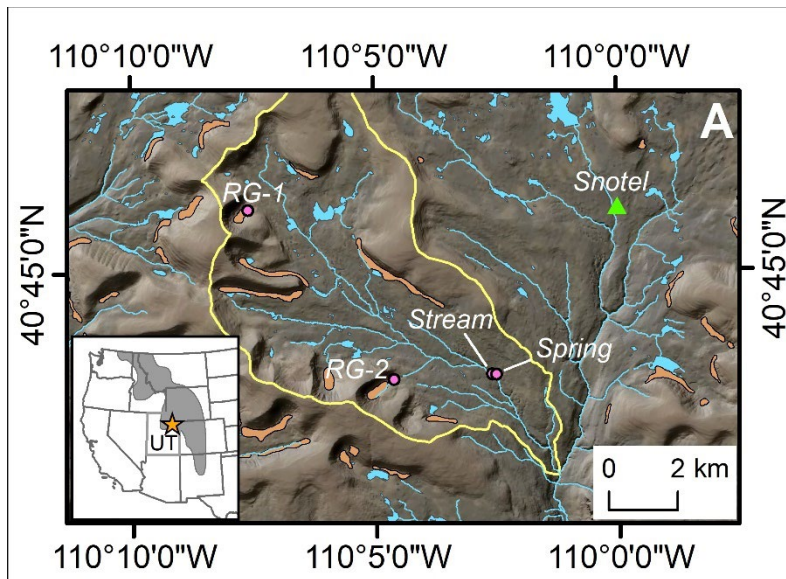
Figure 1: Location Map of the study area. Inset shows location of the Uinta Mountains (orange star) within the state of Utah (UT). Gray shaded polygon represents the Rocky Mountains. Map presents the upper Whiterocks River watershed (yellow boundary), mapped rock glaciers (orange), the locations of the RG-1, RG-2, Stream, and Spring water samplers (pink circles), and the Chepeta SNOTEL site (green triangle).

3 Methods

This project centered on the collection of time series of water samples using automated samplers outfitted with a carousel of 24 bottles. The samplers were deployed with a solar powered battery system, allowing them to run throughout the summer. To reduce the possibility of isotopic fractionation related to evaporation, sample bottles were modified following published methodology (von Freyberg et al., 2020). In each location, the samplers were deployed in a position higher than their intake to facilitate free draining of the intake hose between samples. The weighted strainer on the end of the water intake line was wrapped in 100-μm nylon mesh to prevent coarse material from clogging the pump. Each sampler was programmed to collect a 45-mL sample twice each day, at midnight and noon. For three days these samples (six samples total) were composited in a single bottle, thus the 24 bottles in each sampler represented a maximum deployment duration of 72 days.

Two samplers were deployed at springs discharging from the base of rock glaciers that were the focus of previous investigations (Munroe, 2018). These features, "RG-1" and "RG-2", are typical of cirque floor, tongue-shaped rock glaciers in the Uinta Mountains (Figures 1 and 2).
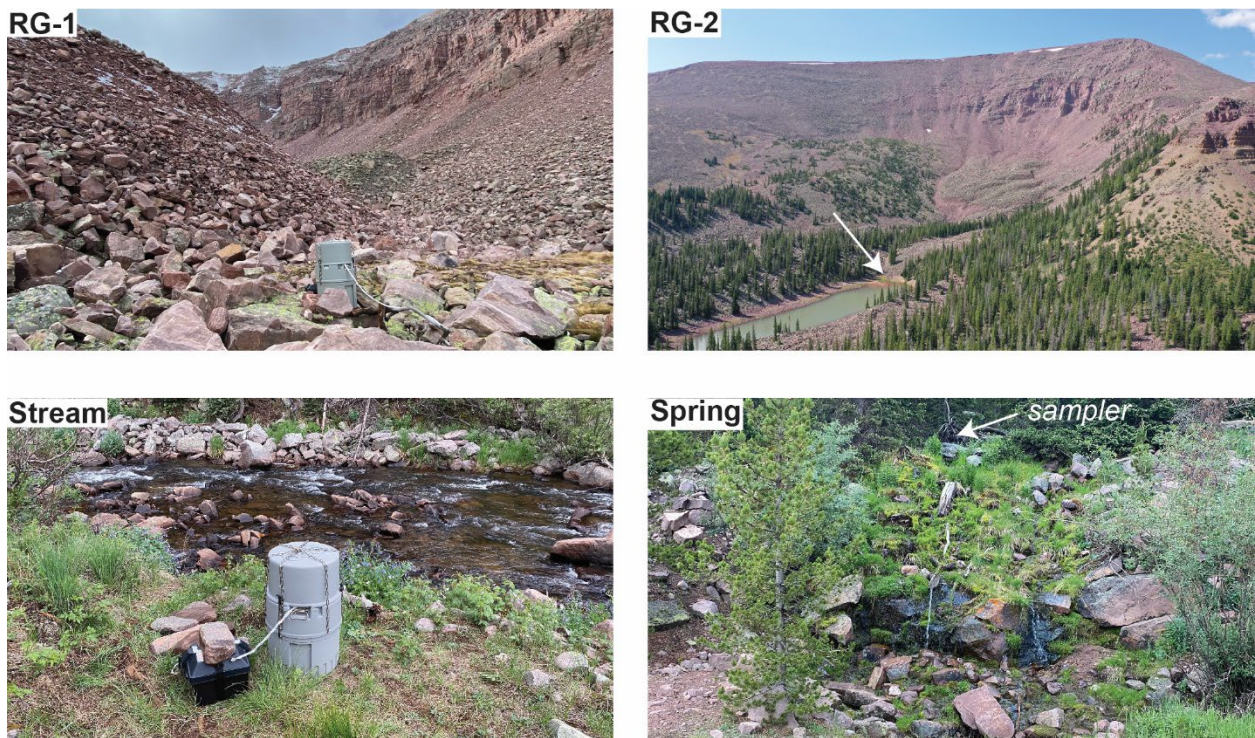
Figure 2: Pictures of water samplers at RG-1, RG-2, the Stream, and the Spring sites.

Each is approximately 600 m long, 100 m wide, and has steep frontal and side slopes standing up to 20 m tall. Fresh exposures on these slopes reveal that the rock glaciers consist of several meters of coarse, openwork boulders overlying a diamicton with a sand matrix. Internal ice is not exposed in either rock glacier, however data loggers reveal that the springs maintain a temperature of 0 °C throughout the summer, and rock glacier surface temperatures

111   equilibrate at -5 °C or colder beneath winter snow cover (Munroe, 2018).   Satellite InSAR (interferometric synthetic

112   aperture radar) analysis indicates that these features move slowly during the winter and accelerate during the

113   summer to velocities of ~10 cm/yr (Brencher et al., 2021).   Collectively these observations suggest the presence of

114   ice within the rock glacier interior.   The spring sampled at RG-1 has a typical summer discharge of 15 L/min.   The

115   discharge at RG-2 was not measured directly, but a water-level logger records diurnal fluctuations of 0.2 (early

116   summer) to 0.02 m (late summer) of the lake into which the spring flows.   Given the surface area of the lake (12,000

117   m^2), these daily variations suggest a discharge on the order of 10^2 to 10^3 L/min.   In both cases these estimates are

118   approximations because much water likely drains belowground through the frost-shattered bedrock and glacial till

119   that mantles the surrounding landscape.

120   Two additional water samplers were deployed at non-rock glacier locations.   The "Spring" sampler

121   collected groundwater discharging from a typical spring unrelated to a rock glacier, and the "Stream" water sampler

122   was positioned slightly upstream along the main channel of the West Fork Whiterocks River, the master stream in

123   this drainage (Figure 1).   These samplers were configured and programmed in an identical manner to those deployed

124   at the rock glacier springs.

125   To constrain the properties of precipitation in the study area, grab samples of snow were collected on the

126   surfaces of RG-1 and RG-2 when the water samplers were deployed.   Water draining from a melting snowbank on

127   RG-2 was also collected.   Rain was collected during the deployment period at the RG-2 and the Spring locations

128   using samplers designed to eliminate evaporation-related fractionation of isotope values (Gröning et al., 2012).

129   Given the sampler design, the rain samples are a composite of all precipitation accumulating during each

130   deployment period.

131   All samplers were installed at the beginning of July, 2021 (Table 1), which was the earliest date at which

132   the study area was accessible due to deep winter snow cover.   At the Stream, Spring, and RG-2 samplers a

133   subsample was taken from the first bottle about a week later, with the remainder left inside the sampler.   It was not

134   possible to revisit the more distant RG-1 sampler at this time.   This procedure provided a check on the potential role

135   of evaporation fractionating the water samples as they waited inside the sampler.   All bottles were emptied at the

136   beginning of September, and the samplers were relaunched to run until mid-October, when they were emptied again

137   and deactivated for the winter.   The two precipitation samplers were emptied when the water samplers were

138   serviced. All samples for stable isotope analysis were filtered in the field to 0.2 μm and stored in 7-ml glass vials

139   with Teflon-lined caps. Samples for ICP-MS analysis were stored in 15-ml centrifuge tubes. These samples were

140   vacuum filtered with Whatman Number 1 paper in the lab and acidified to pH 2 with trace-element grade HNO_3. In

141   a preliminary phase of this project, daily samples were also collected at RG-2 in the fall of 2020.

Table 1. Locations, Dates, and Durations of Water Sampler Deployments							
Sampler	Latitude	Longitude	Elevation (m)	Deployed	Emptied	Emptied	Duration (Days)
RG-1	40.766906	-110.127608	3408	7/2/2021	9/5/2021	10/7/2021	97
RG-2	40.721883	-110.076875	3197	7/1/2021	9/2/2021	10/6/2021	97
Spring	40.723016	-110.042131	2977	7/3/2021	9/2/2021	10/6/2021	95
Stream	40.722979	-110.043123	2965	7/3/2021	9/6/2021	10/6/2021	95

Stable isotope measurements were made with a Los Gatos 45-EP Triple Liquid Water Isotope Analyzer at Middlebury College. Samples were run against a bracketing set of 5 standards and calibrated with a cubic spline function. Each sample was analyzed 10 times, with the first 2 injections discarded to minimize cross-over. Standards were run as unknowns after every five samples as an internal check on the results. Accuracy of the instrument is 0.4‰ for δD and 0.1‰ for $\delta^{18}O$. The standard deviation of repeat injections of the samples in this study was 0.17‰ for δD and 0.04‰ for $\delta^{18}O$. Results were compared with the Global Meteoric Water Line-GMWL (Craig, 1961) as well as a Local Meteoric Water Line (LMWL) estimated from OIPC, the Online Isotopes in Precipitation Calculator (Bowen and Wilkinson, 2002; Bowen and Revenaugh, 2003). Values of *d-excess* were calculated as *d-excess* = $\delta D-(8*\delta^{18}O)$ (Dansgaard, 1964).

Hydrochemical characterizations were made with a Thermo iCap ICP-MS at Middlebury College. Samples were run against a set of standards derived from NIST Standard Reference Material 1643f "Trace Elements in Water". An in-house standard was used to determine the abundance of Si and Ti, which are not present in 1643f. The NIST standard and the in-house standards were run after every 10 unknowns and a linear correction was applied to compensate for instrument drift. Interpretation focused on elements that consistently exhibited concentrations >1 ppb.

4 Results

In total, 141 water samples were analyzed, consisting of 134 samples from the four time-series, 4 samples of rain, 2 samples of snow, and 1 sample of snowmelt. The time-series are essentially complete with no gaps between early July and mid-October. The lone interruption is one bottle from the Stream sampler, representing 18-20 July, that was empty, apparently because the river level briefly dropped below the intake hose.

Overall values of δD in the time-series range from -118.94 to -83.71‰. Values of $\delta^{18}O$ range from -16.36 to -12.24‰, and $\delta^{17}O$ from -9.13 to -6.39‰ (Table 2). The mean of δD is lowest in the Spring samples (-113.44‰) and highest at RG-1 (-91.24‰). The same pattern holds for mean values of $\delta^{18}O$ and $\delta^{17}O$ (Table 2). Values of *d-excess* are highest at the RG sites, and lowest (~10‰) in the Stream (Table 2). Values of δD and $\delta^{18}O$ for the subsamples from the first bottle in the Stream, Spring, and RG-2 samplers are quite similar to the remainder that was left in the collector through the summer (Figure 3).
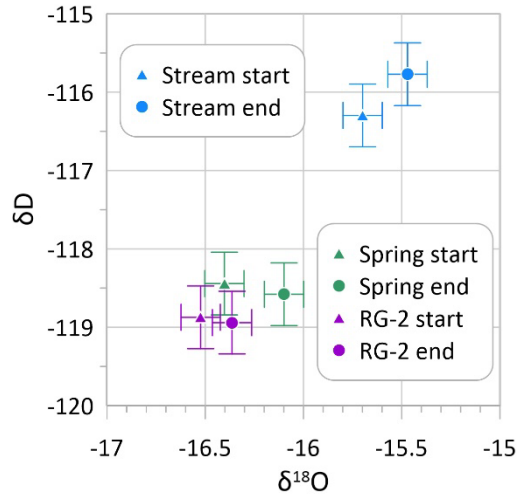
Figure 3: Comparison of isotope values measured for samples from RG-2, the Stream, and the Spring samplers. Subsamples were removed from the first sample in early July and the remainder of the water was left inside the collector until early September. Analysis of the sample pairs confirms that potential evaporation-related fractionation was minimal.

180

Table 2: Isotope Values for Water Samples				
	δ^2H	$\delta^{18}O$	$\delta^{17}O$	d-Excess
	(‰)	(‰)	(‰)	(‰)
Stream (n=31)				
Mean	-103.86	-14.17	-7.38	9.52
Median	-102.55	-13.90	-7.40	9.02
Standard Deviation	4.92	0.57	0.31	1.52
Minimum	-115.77	-15.47	-8.06	7.97
Maximum	-97.05	-13.52	-6.78	12.62
Spring (n=33)				
Mean	-113.44	-15.57	-8.80	11.16
Median	-113.59	-15.60	-8.84	10.79
Standard Deviation	3.25	0.42	0.20	1.03
Minimum	-118.58	-16.12	-9.13	9.57
Maximum	-103.35	-14.28	-8.30	13.80
RG-1 (n=33)				
Mean	-91.24	-13.13	-6.94	13.83
Median	-87.22	-12.80	-6.62	13.87
Standard Deviation	8.52	0.88	0.60	2.59
Minimum	-113.35	-15.67	-8.48	9.80
Maximum	-83.71	-12.24	-6.39	20.82
RG-2 (n=34)				
Mean	-101.32	-14.53	-7.52	14.93
Median	-98.27	-14.24	-7.19	15.50
Standard Deviation	7.46	0.79	0.58	1.32
Minimum	-118.94	-16.36	-8.76	11.97
Maximum	-89.99	-13.10	-6.92	16.91

Values of δD and $\delta^{18}O$ are linearly and significantly (p<0.001) related with a slope of 8.8 and a Y-intercept of 24.4‰ (Figure 4). Lower values of $\delta^{18}O$ plot closer to the GMWL; higher values of $\delta^{18}O$ plot increasingly above the GMWL. Plotting the data from the individual samplers separately, with color coding by month, reveals additional details (Figure 5). Values for the Stream and Spring samplers plot along the GMWL through the summer. For the Stream, the lowest values are from July with higher values in late summer and fall. For the Spring, the lowest values are again July, with the highest values in August; September and October values fall in between (Figure 5). For the two rock glaciers, July values are low and closer to the GMWL, but values from late summer and the fall plot notably above the GMWL with *d-excess* up to 20‰. At RG-2, a similar pattern was noted in daily

190   samples collected during September, 2020 (Figure 5). Figures 4 and 5 also illustrate that isotope values are

191   significantly more depleted at RG-2 compared with RG-1.

192
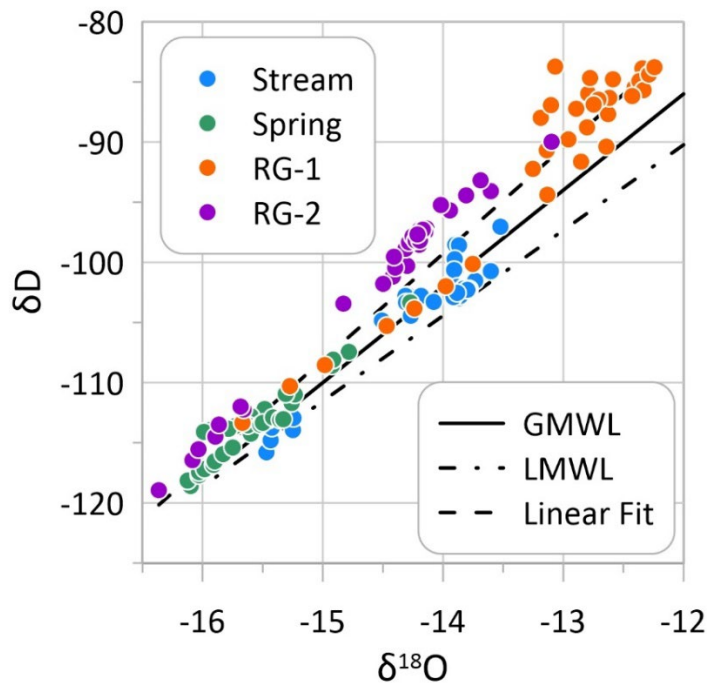
Figure 4: Dual isotope plot of $\delta^{18}O$ and δD for the samples collected at RG-1, RG-2, the Stream, and the Spring.
The Global Meteoric Water Line (GMWL), a local meteoric water line (LMWL) determined from the Online
Isotopes in Precipitation Calculator (Bowen and Wilkinson, 2002; Bowen and Revenaugh, 2003), and a linear fit to
the data are presented for reference.

197   Plotting the data from the different samplers as time-series reveals patterns in the evolution of isotope

198   values during the sampling period (Figure 6). Given the strong correspondence between values of δD and $\delta^{18}O$,

199   only $\delta^{18}O$ is presented for clarity. Values are low at the start of the sampling period (early July), and generally rise

200   in all records through the summer and early fall (Figure 6A). The Spring and RG-2 both start below -16‰; the

201   Stream and RG-1 start slightly higher, near -15.5‰. All of the records exhibit transient spikes to less negative

202   values that occur quickly and taper gradually back to background levels (Figure 6A). These spikes align with pulses

203   of precipitation recorded at the Chepeta SNOTEL (snowpack telemetry) site <10 km to the north, and at a similar

204   elevation (Figure 1). Thus, it is likely that they represent rainstorms that delivered water less depleted in $\delta^{18}O$

205   relative to SMOW, a response reported in other studies (Krainer and Mostler, 2002). After these pulses are removed

206   from the data to highlight the background trends at each of the sites (Figure 6B), the record from the Spring is seen

207   to be the most stable, with nearly all values between -16 and -16.5‰. The water at RG-2, which started off similar

208   to the Spring, rises steadily to a maximum of -14‰ in early October. The Stream rises from -15.5‰ to -14‰ by the

209   third week of August, and stabilizes through the end of the record. Finally, RG-1, which also starts at -15.5‰, rises

210   rapidly in the first half of July, then more gradually until early September, when it peaks at -12.5‰ before dropping

211   to -13‰.
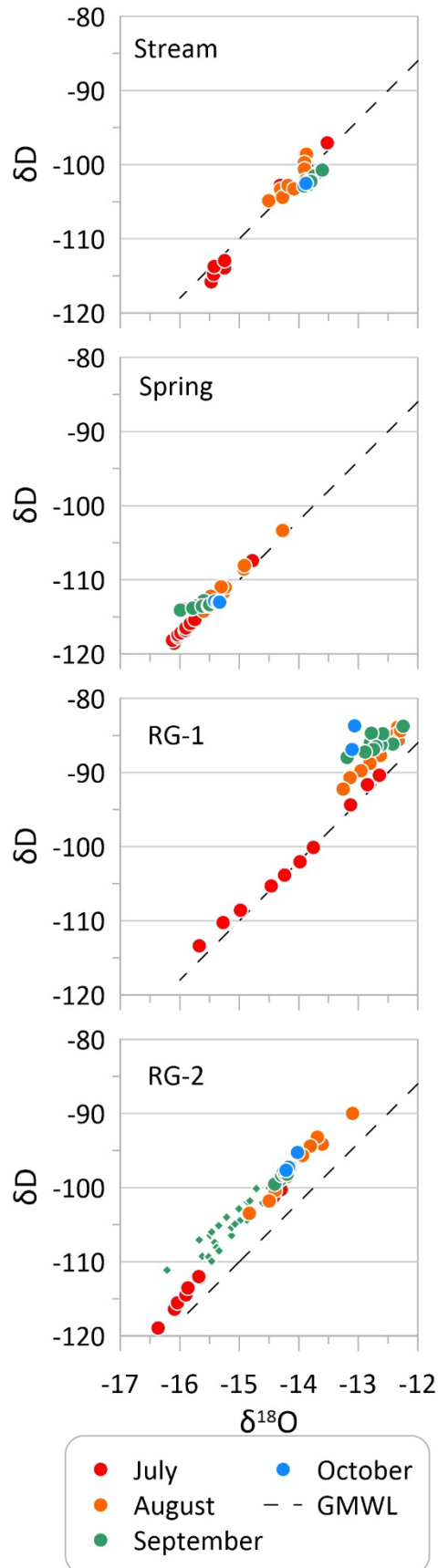
Figure 5: Dual isotope plots for the four individual time series. Color-coding represents the month of sample collection. The tendency for samples at the Stream and Spring to remain on the waterline while samples from the rock glaciers deviate to higher values of *d-excess* in late summer and fall is clearly evident. Green diamonds for RG-2 present reconnaissance data from September, 2020.
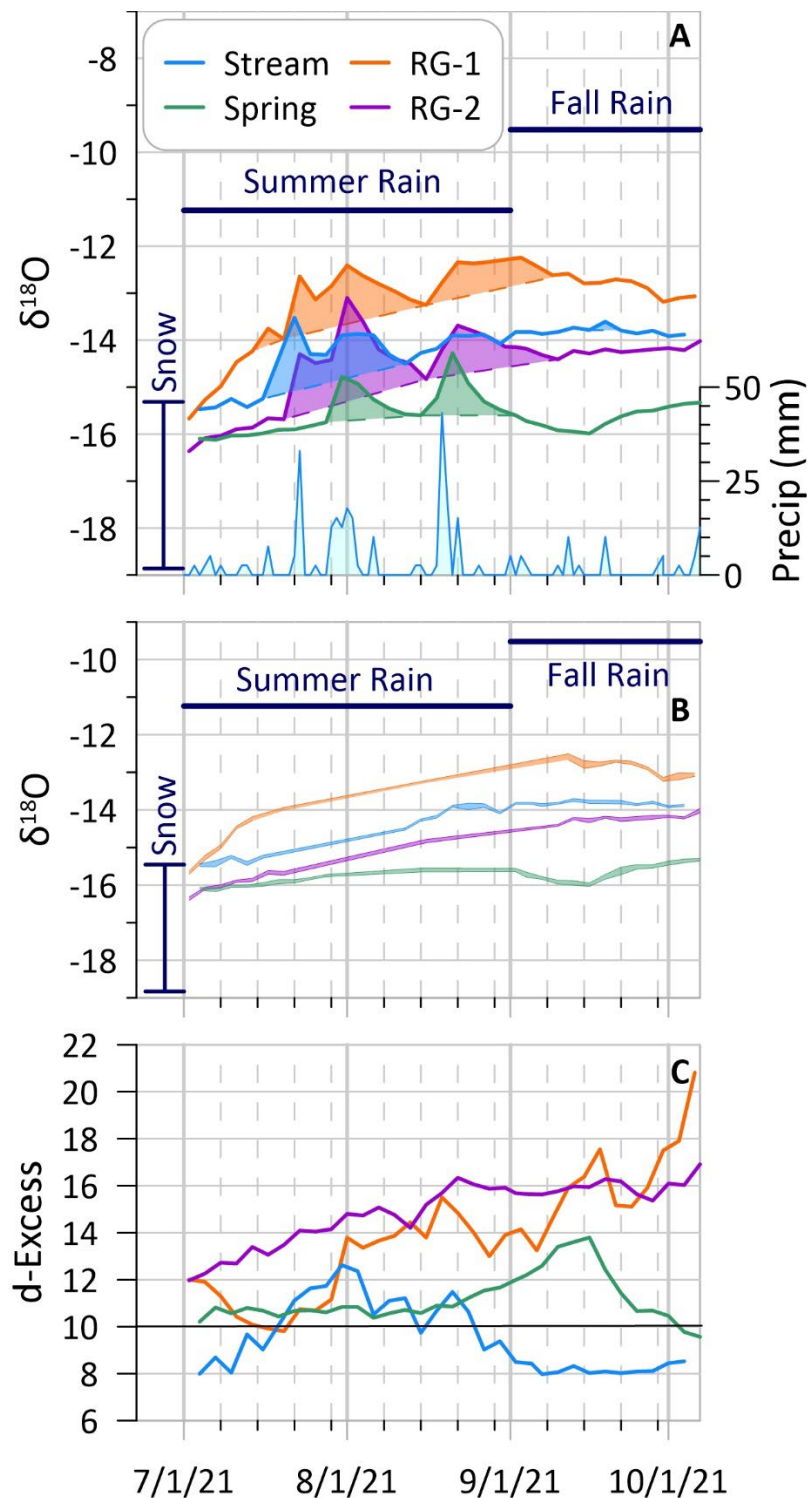
Figure 6: Time series from the four sampling sites. (A) Values of $\delta^{18}O$ presented along with average values for snow and rain, and daily precipitation recorded at the Chepeta SNOTEL site (Figure 1). (B) Same as Panel B with transient spikes in $\delta^{18}O$ due to precipitation events removed. Line width represents ± 1 standard deviation. (C) Times series of *d-excess*. The reference value of 10‰ is highlighted.

245   Values of *d-excess* in the time-series exhibit varying patterns (Figure 6C). Values from the Stream initially rise,

246   then fall through August and stabilize at 8‰ in the fall. The Spring samples are initially stable between 10 and

247   11‰, then rise in early September to a high of 14‰, before falling back to 10‰. The two rock glaciers sites, in

248   contrast, rise steadily from near 10‰, to ≥17‰ in early October (Figure 6C).

249   Context for the isotope values from the water samplers is provided by the precipitation samples collected at

250   the Spring and RG-2 sites, and grab samples of snow from RG-1 and RG-2 (Figure 6). Values of $\delta^{18}O$ in

251   composited July and August precipitation at the Spring and RG-2 sites average -11.2‰, and fall precipitation

252   averages -9.5‰. Values of $\delta^{18}O$ in snow samples are lower, averaging -17‰ (with *d-excess* ~10‰) with a range

253   from -15.3 to -18.6‰. This wide range is not surprising given that the stable isotopic composition of snow can vary

254   spatially across complex mountain terrain (Dietermann and Weiler, 2013), and can evolve through winter

255   sublimation and the process of snowpack melting (Taylor et al., 2001; Unnikrishna et al., 2002; Earman et al., 2006;

256   Lechler and Niemi, 2011). Nonetheless, these measurements are consistent with other reported snow samples from

257   the Uintas (Munroe, 2021) and with values predicated by the OIPC (Bowen and Wilkinson, 2002; Bowen and

258   Revenaugh, 2003). Thus, they are considered to provide a reasonable constraint on the isotopic composition of

259   snow within the study area.

260   Hydrochemical analysis with ICP-MS reveals 12 elements that are consistently detectable in these samples:

261   Ba, Ca, Fe, K, Mg, Mn, Na, Ni, Rb, Si, Sr, and Ti. Ca and Si are generally the most abundant cations, with mean

262   abundance ~1500 to 2000 ppb, followed by K, Na and K with abundances averaging 500-800 ppb. Fe and Ba are

263   generally present at abundances around 100 ppb; other elements are present at lower concentrations (Table 3).

264   Principal component analysis of these elemental concentrations, conducted with a varimax rotation, places five

265   elements (Ba, Ca, Na, Mg, Ni) on the first component (PC-1), with Ti, Rb, Si, K, Sr, and and Mn on the second (PC-

266   2). Together these two components explain 78% of the variance. Highest values of PC-1 are found in the Spring

267   samples, followed by the Stream and the two rock glaciers. In contrast, PC-2 is highest at the rock glacier sites and

268   lower in the Stream and Spring. Plotting of PC-1 vs. PC-2 reveals a nearly complete separation between the rock

269   glacier water and samples from the Stream and Spring (Figure 7). When considered as time-series, values of both

270   components are generally stable at the Stream and Spring, but rise consistently through the summer and fall at RG-1

271   and RG-2 (Figure 8).

272   The same 12 cations were generally detectable in the precipitation samples, with the exception of Fe, which

273   was typically below the detection limit. Values of Na, K, Mn, Rb, Fe, Ni, and Sr were higher in snow samples

274   relative to rain, with particularly high values of Na and K in the July snow sample from the RG-2 site (Figure 9). In

275   contrast, Ca, Ti, Ba, Mg, and Si were more abundant in rain samples. All elements were less abundant in rain than

276   in the time-series.

277

278   **5 Discussion**

279   **5.1 Isotopes and Hydrochemistry**

280   The automated samplers utilized in this project were successful at collecting essentially uninterrupted sequences of

281   water throughout their deployment. Modification of the samplers effectively reduced evaporation-related

282   fractionation that could have skewed the results over the long duration deployments. As seen in Figure 3, analysis

283   of the subsample from the first sample bottle that was removed in early July yielded similar results to the water that

284   remained inside the sampler until September.   Values of δD and $\delta^{18}O$ overlap within error for RG-2 and are very

Table 3: Summary Hydochemistry

	Na (ppb)	K (ppb)	Ca (ppb)	Ti (ppb)	Mn (ppb)	Rb (ppb)	Ba (ppb)	Mg (ppb)	Si (ppb)	Fe (ppb)	Ni (ppb)	Sr (ppb)
Stream (n=31)												
Mean	848.2	465.8	1636.9	3.2	3.9	0.4	64.6	496.0	1053.2	66.9	0.8	9.0
Median	790.0	347.3	1635.9	3.2	2.4	0.3	61.6	499.7	1056.7	49.3	0.6	9.0
Standard Deviation	199.6	393.4	77.9	0.3	4.7	0.1	8.9	17.2	79.9	80.0	0.4	0.9
Minimum	605.4	262.6	1471.5	2.5	0.7	0.2	56.2	451.5	866.0	0.0	0.2	7.7
Maximum	1325.4	2264.8	1836.5	4.2	23.2	0.9	92.3	528.9	1176.2	410.1	1.6	11.2
Spring (n=33)												
Mean	1075.5	499.9	1997.5	4.4	3.3	0.3	115.6	599.0	2034.7	34.7	0.7	11.0
Median	1104.8	513.1	1860.8	3.9	3.2	0.3	104.2	579.6	2048.8	20.1	0.5	10.8
Standard Deviation	284.8	107.3	313.0	0.9	1.6	0.1	34.9	56.8	84.4	33.6	0.6	1.1
Minimum	685.5	306.8	1764.4	3.6	1.1	0.2	90.7	517.4	1816.1	7.3	0.2	9.0
Maximum	2147.7	877.6	3100.8	7.5	6.7	0.7	251.1	770.6	2204.3	164.1	2.9	14.1
RG-1 (n=33)												
Mean	619.8	612.0	1587.5	12.5	12.3	1.2	53.6	527.9	2265.6	277.3	0.7	12.3
Median	633.4	602.9	1550.2	11.5	4.3	1.1	52.6	506.7	2145.7	234.1	0.7	11.7
Standard Deviation	123.5	207.3	396.4	6.3	30.8	0.7	18.8	132.0	1008.7	215.0	0.4	4.3
Minimum	380.9	259.0	938.2	3.5	1.4	0.2	27.7	309.0	678.5	18.1	0.1	5.6
Maximum	898.9	1081.6	2527.2	25.8	173.6	2.6	120.5	830.7	4108.3	1041.1	1.8	20.8
RG-2 (n=34)												
Mean	573.6	388.7	1289.7	6.1	8.1	0.7	43.3	396.9	1301.1	127.7	0.3	7.6
Median	570.9	372.2	1257.2	4.8	2.7	0.5	36.9	380.0	1225.0	56.3	0.2	7.0
Standard Deviation	170.6	95.0	257.4	4.1	14.2	0.4	17.3	87.3	444.9	174.2	0.3	2.7
Minimum	338.7	249.0	852.3	1.3	0.4	0.1	23.9	266.7	568.9	0.0	0.0	3.7
Maximum	883.8	592.8	1849.8	22.5	60.6	2.0	95.4	621.9	2323.0	764.2	1.8	15.1

285
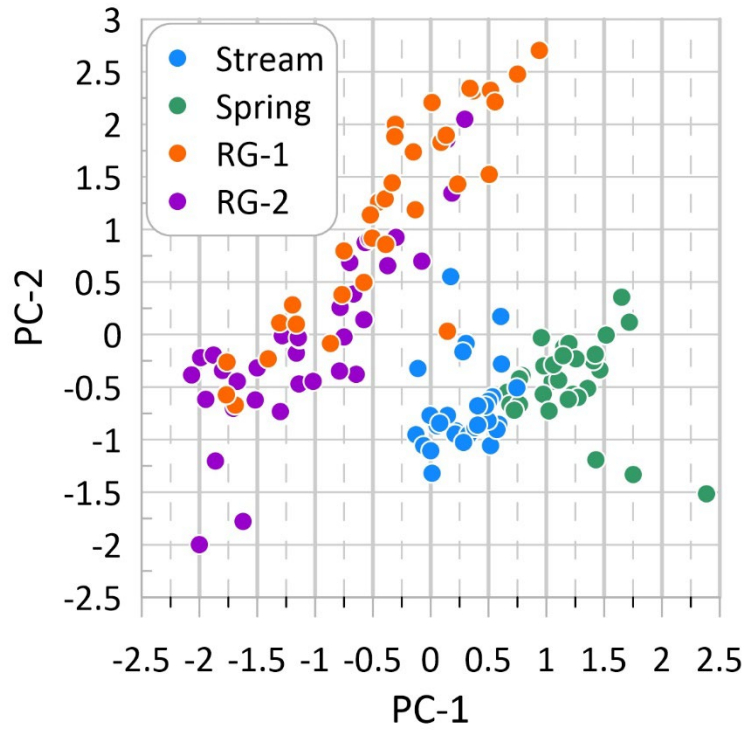
Figure 7: Biplot of the first and second principal components determined for major elements in the water samples. The similarity of the rock glacier water samples is clear, as is their lack of overlap with the Stream and Spring samples.

300
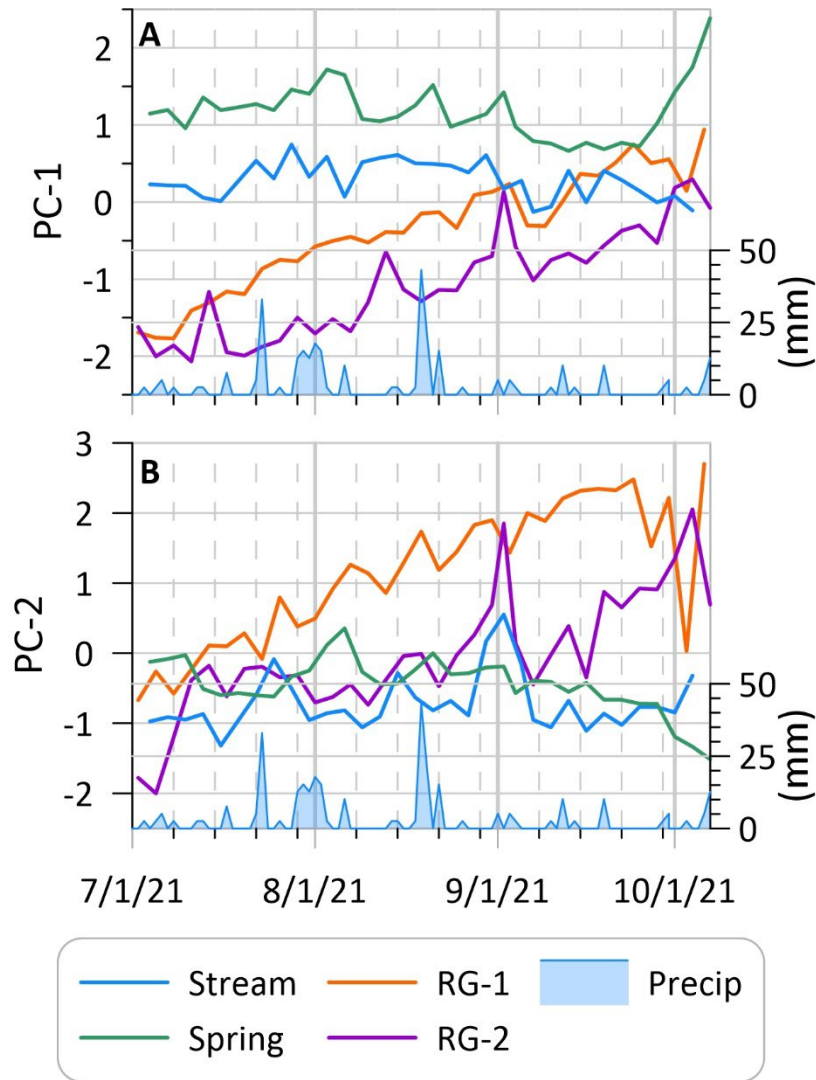
Figure 8: Time series of the first and second principal components presented in Figure 7. Values tend to be stable through the melt season at the Stream and Spring, but rise notably at both the rock glacier sites.

303

close for the Stream and Spring. There is a slight increase in $\delta^{18}O$ of ~0.2‰ over the course of the summer, which could indicate evaporation, however this shift is far less than the changes observed in these sequences of samples from start to finish. Thus, the time-series are interpreted without significant concern that values were altered by evaporation.

The sampling and analysis strategy in this project was designed to evaluate whether water draining from representative rock glaciers in the Uinta Mountains differs from streamwater and groundwater in a manner that is consistent with the presence of melting ice within the rock glacier. The summer of 2021 was a particularly appropriate time to attempt this because the snowpack during the preceding winter was notably below average. On
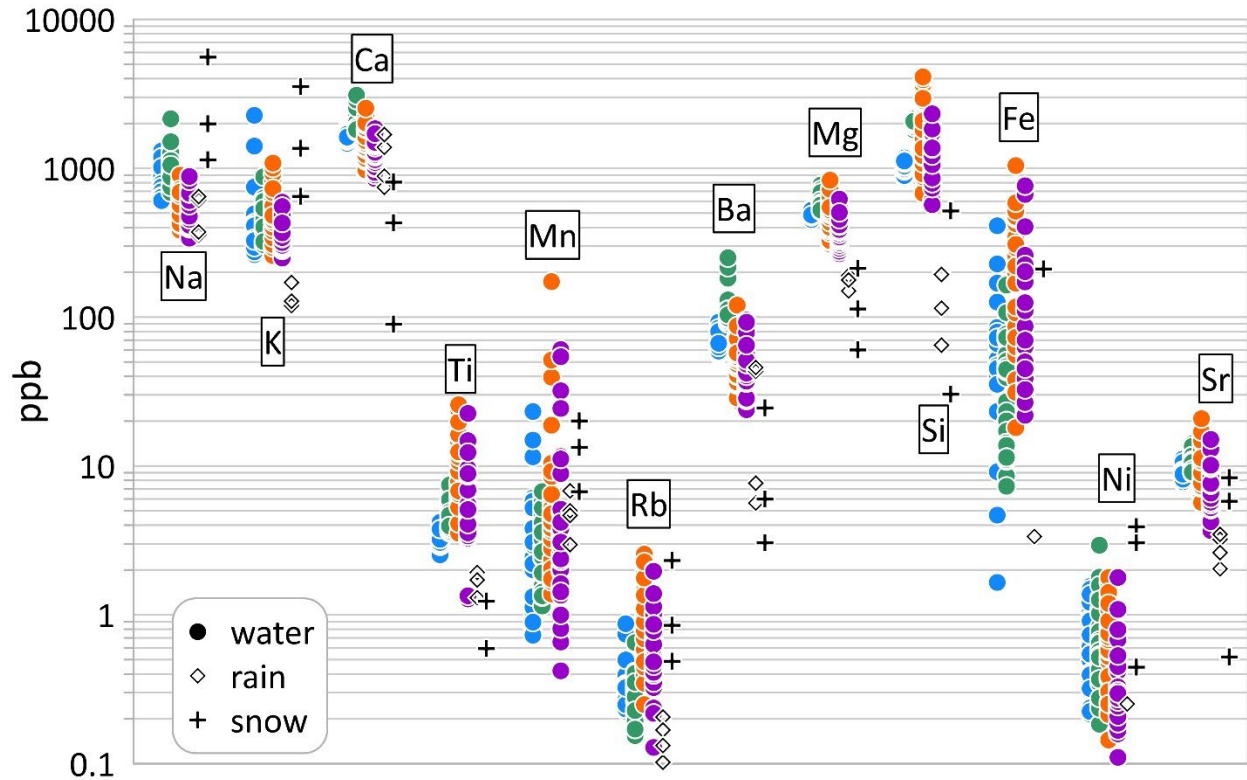
312
313 **Figure 9**: Abundances of detectable elements in the time series of water samples, along with the rain and snow
314 samples. Water samples are presented from left to right with the same color designations as previous figures: Blue =
315 stream, Green = Spring, Orange = RG-1, and Purple = RG-2. Note the logarithmic scale on the Y-axis.

316 April 1, 2021 the Chepeta SNOTEL (Figure 1) was at 83% of the 1991-2020 median of 380 mm snow water

317 equivalent (SWE), but by April 13, the average date of the annual peak, SWE was just 52% of average (188 mm).

318 In contrast to other years in which we have conducted fieldwork at the RG-1 and RG-2 sites, the surfaces of the rock

319 glaciers were notably snow free when the samplers were deployed in early July. Inspection of high-resolution

320 satellite imagery confirms that visible snow on the rock glacier surfaces disappeared by the end of June, and that

321 essentially no snow was present in the West Fork Whiterocks Drainage after the start of July. Therefore, it is

322 unlikely that the water collected at RG-1 and RG-2, particularly late summer and fall, was sourced from melting

323 snow.

324 Analysis of stable isotopes reveals contrast between the water types that can be linked back to their sources

325 and flowpaths. Groundwater from the spring exhibits the most depleted $\delta^{18}O$, with values similar to the snow

326 samples (Figure 6). The snow samples span a relatively wide range of $\delta^{18}O$, but they are the most negative

327 measured in this study, thus this correspondence suggests that the groundwater system is primarily recharged by

328 snowmelt. The average annual maximum SWE at the Chepeta SNOTEL station of 380 mm equals half of the mean

329 annual precipitation. The snowmelt pulse in the spring, therefore, is apparently the only precipitation event of the

330 year that can overwhelm the moisture holding capacity of the soil and pass water into the groundwater system. The

331 low $\delta^{18}O$ values of the water discharging from the spring during the course of the summer, despite numerous

332 rainstorms delivering isotopically less depleted water, emphasizes that the deeper groundwater system is snow-

333 dominated and stable.

334   Samples from RG-1 and RG-2 from July plot on the GMWL, with low values of δD and δ^{18}O consistent

335 with a large component of snowmelt (Figure 5), which is isotopically depleted in this study and in values reported

336 from elsewhere in the Uintas (Munroe, 2021). Even though visible snow was absent from the rock glacier surfaces

337 at this time, this correspondence indicates that snow was still melting within the interstices between blocks on the

338 rock glacier surface, a situation that was reported by previous work (Krainer et al., 2007). By the beginning of

339 August, however, isotope values at both rock glacier springs depart from the GMWL and rise to higher values of *d-*

340 *excess* (Figure 5). This pattern is not seen in the Spring or the Stream time-series, which remain on the GMWL from

341 start to finish. Thus, late summer and fall water discharging from both rock glaciers is distinct from contemporary

342 precipitation and groundwater. This pattern is particularly dramatic at RG-1, where all of the August through

343 October samples cluster around a δ^{18}O of -13‰ with *d-excess* values as high as 20‰. Previous work on rock

344 glacier hydrology has reported high values of *d-excess* in late-summer rock glacier discharge, and interpreted them

345 as a signal of melting internal rock glacier ice that has undergone numerous freeze/thaw cycles (Steig et al., 1998;

346 Williams et al., 2006).

347   The time-series of PC values reinforce the uniqueness of the rock glacier water. Values for the Spring and

348 for the Stream are notably stable through the melt season (Figure 8). This consistency suggests that these systems

349 are not directly impacted by short-term events like rainstorms, or even changes over seasonal timescales,

350 presumably due to their well-mixed nature and large volumes. In contrast, the time series for the two rock glacier

351 springs exhibit a dramatic rise. Values of PC-1 increase starting at the beginning of July in both records; values of

352 PC-2 start rising in July for RG-1 and in mid-August for RG-2. Concentrations for many elements increase by a

353 factor of 3 or more from early July until October. This enrichment is consistent with movement of water through the

354 fine matrix of crushed rock material in the rock glacier interior, where fresh mineral grains are available for rapid

355 chemical weathering by cold water charged with carbonic acid (Krainer and Mostler, 2002; Williams et al., 2006).

356 Melting of ice would both liberate meltwater and open flowpaths through this material. The pattern of rising

357 dissolved load through the summer, therefore, provides additional support for the interpretation that the source of the

358 water draining from the rock glaciers shifts after snowmelt is over.

359   The transition in source of the water draining from the rock glaciers is further illustrated by biplots of δ^{18}O

360 against Ca and Mg content (Figure 10). Values for average snow, rain, and the last sample from each rock glacier

361 define a triangle entirely enclosing samples collected from the rock glaciers. Water draining from the rock glaciers

362 in July exhibits a clear snowmelt influence, but this diminishes in August as the water becomes a more even mixture

363 of rain and rock glacier water. Through September into October, this balance shifts away from rain, eventually

364 reaching a minimal rain contribution in the last water discharged before the system froze up for the winter. Even

365 considering the inherent uncertainty imparted by the small number of precipitation samples, it is obvious that the

366 rock glacier water composition evolves away from snow and rain over the course of the melt season (Figure 10).

367   Williams et al. (2006) proposed a model for changing flowpaths and water sources over the course of the

368   melt season that is relevant for interpreting the results presented here. In early summer, the interior of a rock glacier

369   is frozen and water derived from snowmelt is discharged after draining through the blocky surface layer and running

370   along the top of the frozen core (Krainer and Mostler, 2002). Later in the summer, snowmelt is finished and

371   seasonal ice within the rock glacier begins to melt, opening flowpaths that bring meltwater into contact with fresh
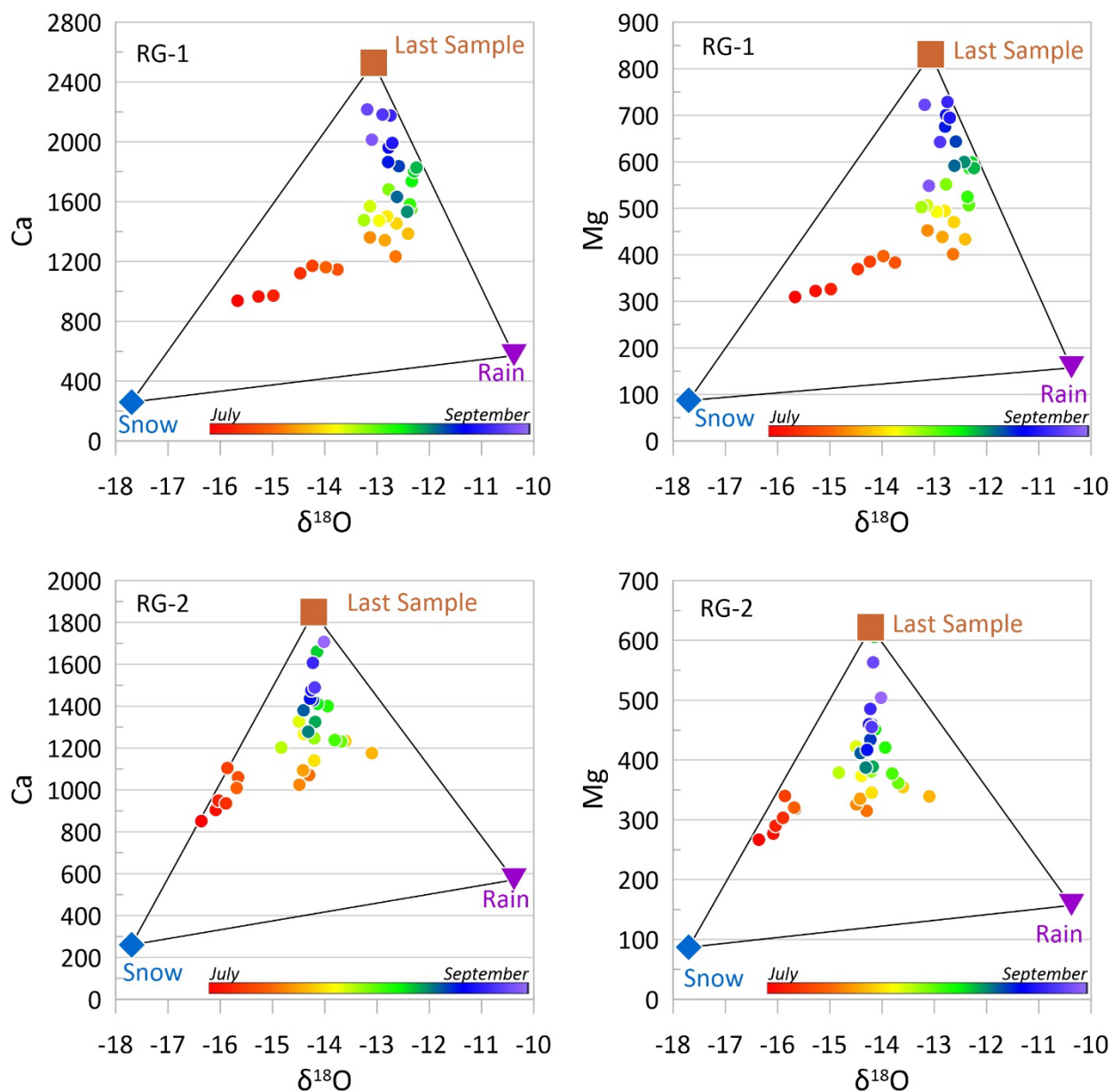
372

373 **Figure 10**: Biplots of $\delta^{18}O$ vs. Ca and Mg at RG-1 and RG-2. Circles represent water discharging from the rock

374   glacier springs, with the rainbow pattern progressing from early July (red) through to early October (purple). The

375   last sample collected at each rock glacier is plotted as the brown square, along with average values for snow and

376   rain. Rock glacier water clearly evolves through the season from a composition dominated by snowmelt, to a

377   mixture of rain and internal water, with decreasing rain influence over time.

378 highly weatherable mineral grains. Finally, in late summer and the fall, older perennial ice within the rock glacier

379 begins to melt (Williams et al., 2007), liberating water with high dissolved load and uniquely high values of *d-excess*

380 due reflecting a history of multiple freeze/thaw cycles. The isotopic and hydrochemical results presented here are

381 consistent with this model, supporting the interpretation that water discharging from Uinta rock glaciers in late

382 summer and fall is derived from the melting of perennial internal ice.

5.2 Implications for High Mountain Hydrology

384 The rock glaciers studied in this project are but two of eight mapped (Figure 1) within the West Fork Whiterocks

385 watershed (Munroe, 2018), which also hosts extensive talus (Munroe and Laabs, 2009) that may contain non-trivial

386 amounts of ice. It is reasonable to predict, therefore, that water derived from rock glaciers may comprise an

387 important amount of the overall streamflow in the latter part of the summer and fall. Figure 11 presents biplots of

388 $\delta^{18}O$ vs. Ca and Mg content, two elements that are notably elevated in the late summer rock glacier water in the

389 Uintas and elsewhere (Williams et al., 2006).

390
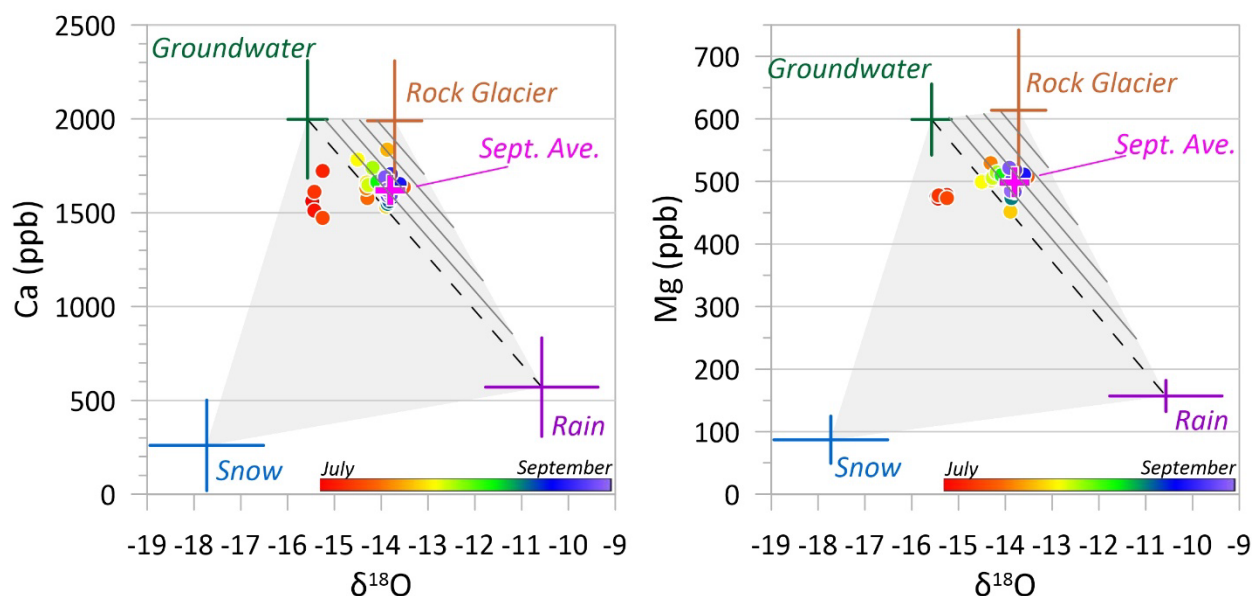
Figure 11: Biplots of $\delta^{18}O$ vs. Ca and Mg used to determine the contribution of rock glacier discharge to
streamflow. Water in the stream is plotted with a rainbow pattern progressing from July (red) through to early
October (purple). Crosses represent the end members of snow, rain, groundwater, and rock glacier water. July
streamwater samples contain a mixture of snowmelt and groundwater, but in August and September, snowmelt is
now longer detectable (samples to right of dashed line). Streamwater samples at this time contain non-trivial
amounts of water derived from rock glaciers, with an average of 25% in September (pink cross). Diagonal black
lines denote the abundance of rock glacier water in increments of 20% for emphasis.

398 After Krainer and Mostler (2002), four end member sources of water to the stream are: groundwater, snow, rain, and

399 rock glaciers. The groundwater end member is constrained for the 2021 melt season by the 33 samples from the

non-rock glacier spring. As noted above, the snow end member is less well constrained, however these samples are nonetheless considered a valid representation of the snow lingering in the Whiterocks River watershed in the summer of 2021. Five samples (two from RG-1 and three from RG-2) collected from the rock glacier springs in October immediately before freeze up represent the rock glacier meltwater end member. Finally, two composite precipitation samples from RG-2 and two from the spring site are available to represent rain falling over the course of the melt season. Close inspection reveals, however, that the concentration of Ca in the Spring sampler is ~3x higher than at RG-2, despite the distance of only 3 km between the two sites. The precipitation sampler at the Spring site is located close to a dirt road though, raising the possibility that dust produced by vehicle traffic raised the Ca content of the water collected at this site. Support for this interpretation is provided by 7 years of unpublished precipitation chemistry (n=79 samples) collected by the USDA-Ashley National Forest in the Uintas. Concentrations of Ca in this dataset average 645 ppb, similar to the value of 570 ppb in the rain from the precipitation sampler at RG-2 and notably less than mean of 1535 ppb at the roadside Spring site. Thus, the precipitation samples from RG-2 alone are taken to represent the rain end member in the stream system for the melt season of 2021.

With this approach, the four end members define a polygon entirely surrounding the streamwater samples (Figure 11). As in the time-series from the individual rock glaciers (Figure 5), a clear transition is notable. July streamwater samples exhibit $\delta^{18}O$ values similar to snowmelt and groundwater. In contrast, late summer and fall samples plot far from the snowmelt end member and entirely within a triangle bounded by the groundwater, rock glacier water, and rain. Within this triangle, although the proportions vary somewhat between samples, individual streamwater samples from August and September can be visually separated as a mixture of ~20-30% rain, ~25 to 75% groundwater, and up to 50% rock glacier water. The overall mean of September streamwater samples can be defined as ~25% rain, ~50% groundwater, and ~25% rock glacier water. Water with a signature similar to that of springs discharging directly from rock glacier termini, therefore, generally makes up approximately one quarter of all the water flowing in the master stream of this drainage after snowmelt has ended.

Given the detectable contribution of rock glacier meltwater to streamflow in this system, it is worth considering whether rock glacier ice is melting at an unsustainable rate. This possibility is hard to evaluate directly, given that mass balance techniques for ice glacier systems are difficult to apply to rock glaciers (Østrem and Brugman, 1966). Nonetheless, it is notable that a depression consistent with subsidence accompanying the melt-out of an ice core is present in the upper part of RG-2 (Figure 12). A high-resolution topographic model constructed for this rock glacier using structure-from-motion applied to images collected with an uncrewed aerial vehicle (UAV) reveals that this depression has an area of 19,350 m^2 and a volume of 106,500 m^3 (mean depth of 5.5 m). If this depression formed due to the loss of ice, this volume corresponds to ~10^8 L of water. At rates of 10^2 to 10^3 L/min estimated for the modern flow, that equates to 70 to 700 days. This calculation is inherently general given the uncertainty around the age and timing of the depression, and the true rates of water discharge. Nonetheless, the presence of this depression and its dimensions suggests that ice within this rock glacier may have begun melting unsustainably in the past few decades in response to rising summer temperatures noted in Uinta climate records

436 (Brencher et al., 2021). Future InSAR monitoring may help constrain subsidence on this and other rock glaciers,

437 yielding additional information about the response of these features to contemporary climate warming and likely

438 changes in their future contributions to high-elevation hydrology.

439

440 **6 Conclusion**

441 Time series of samples collected during the summer of 2021 reveal that water draining from rock glaciers in the

442 Uinta Mountains of Utah (USA) has a composition distinct from groundwater and from water in the master stream
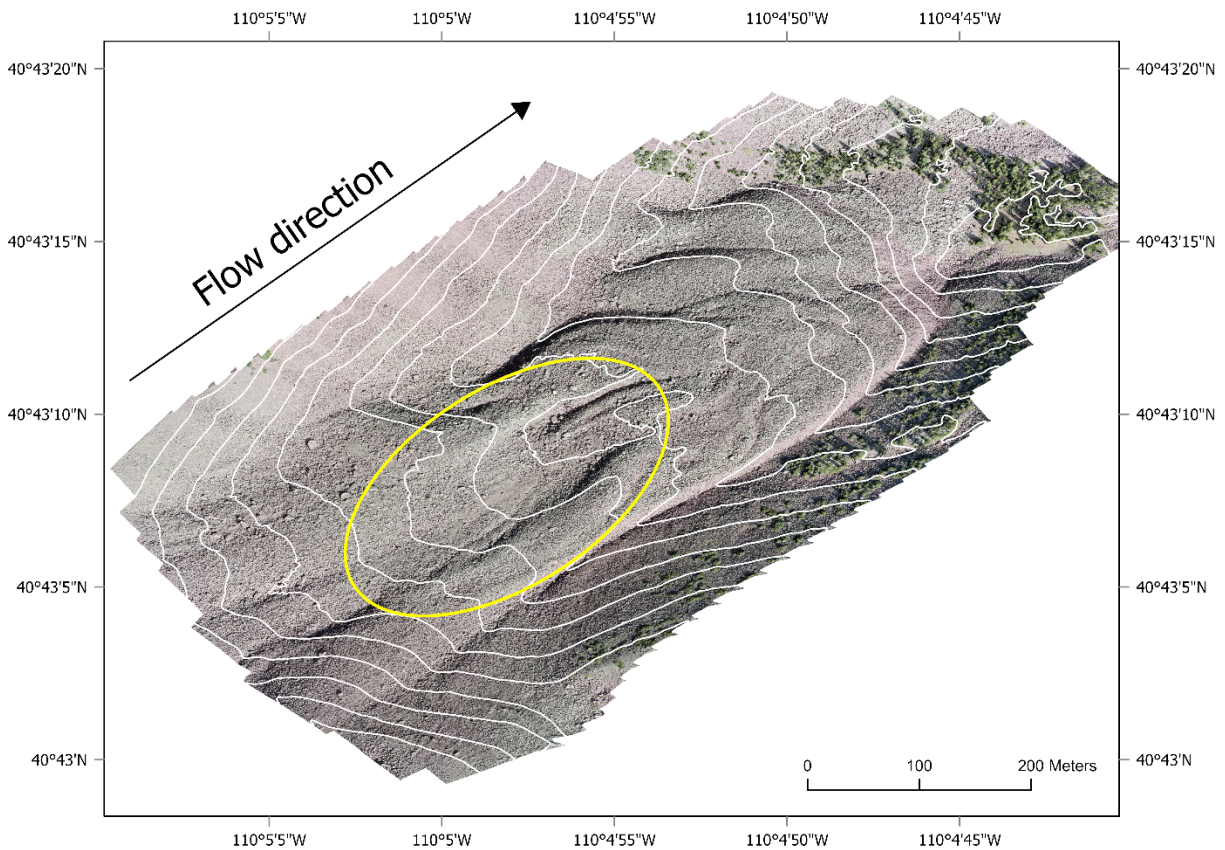
443

444 **Figure 12**: True-color hillshaded photomosaic of RG-2 produced by structure from motion (SfM) applied to a set of

445 243 images collected at an altitude of 120 m above the ground. White lines represent 10-m contours and the black

446 arrow designates the downslope flow direction. The yellow oval highlights the prominent depression near the head

447 of the rock glacier, which may reflect subsidence due to ice meltout.

448

449 of a representative 5000-ha drainage. Rock glacier water resembles snowmelt in the early summer, but transitions to

450 higher values of *d-excess* and greatly elevated Ca and Mg content as the melt season progresses. This pattern is

451 consistent with models describing a change in water source from snowmelt, to melting of seasonal ice, to melting of

452 deeper perennial ice in the rock glacier interior in late summer and fall. Water derived from this internal ice appears

453 to have been the source of ~25% of the streamflow in this study area during September of 2021. This result

454 emphasizes the significant role that rock glaciers can play in the hydrology of high-elevation watersheds,

455 particularly in melt seasons following a winter with below average snowpack.

456

Data Availability

458 The stable isotope and hydrochemical data generated in this study are available in the Hydroshare data repository at

459 http://www.hydroshare.org/resource/2db20d7810254489b14984ef282951e1

460

Author Contributions

462 JM designed the project, conducted the fieldwork and laboratory analyses, interpreted the results, and drafted the

463 figures. JS prepared the manuscript with contributions from AH.

464

465 **Competing Interests**: The authors declare that they have no conflict of interest.

466

Acknowledgements

468 This work was supported by NSF HS-1935200 to PIs Munroe and Handwerger, and NSF MRI-1918436 to Munroe.

469 The authors thank Q. Brencher, C. Kluetmeier, S. Lusk, E. Norris, A. Santis, and A. Takoudes for their assistance in

470 the field, and E. McMahon for help preparing the water samplers.

References Cited

Adler, C., Huggel, C., Orlove, B., and Nolin, A., 2019, Climate change in the mountain cryosphere: impacts and responses: Regional Environmental Change, v. 19, p. 1225–1228.

Albrich, K., Rammer, W., and Seidl, R., 2020, Climate change causes critical transitions and irreversible alterations of mountain forests: Global change biology, v. 26, p. 4013–4027.

Alexander, J.M., Chalmandrier, L., Lenoir, J., Burgess, T.I., Essl, F., Haider, S., Kueffer, C., McDougall, K., Milbau, A., and Nuñez, M.A., 2018, Lags in the response of mountain plant communities to climate change: Global change biology, v. 24, p. 563–579.

Atwood, W.W., 1909, Glaciation of the Uinta and Wasatch mountains: US Government Printing Office, v. 61.

Azócar, G.F., and Brenning, A., 2010, Hydrological and geomorphological significance of rock glaciers in the dry Andes, Chile (27–33 S): Permafrost and Periglacial Processes, v. 21, p. 42–53.

Beniston, M., Farinotti, D., Stoffel, M., Andreassen, L.M., Coppola, E., Eckert, N., Fantini, A., Giacona, F., Hauck, C., and Huss, M., 2018, The European mountain cryosphere: a review of its current state, trends, and future challenges: The Cryosphere, v. 12, p. 759–794.

Biskaborn, B.K. et al., 2019, Permafrost is warming at a global scale: Nature Communications, v. 10, p. 264, doi:10.1038/s41467-018-08240-4.

Bonfils, C., Santer, B.D., Pierce, D.W., Hidalgo, H.G., Bala, G., Das, T., Barnett, T.P., Cayan, D.R., Doutriaux, C., and Wood, A.W., 2008, Detection and attribution of temperature changes in the mountainous western United States: Journal of Climate, v. 21, p. 6404–6424.

Bowen, G.J., and Revenaugh, J., 2003, Interpolating the isotopic composition of modern meteoric precipitation: Water Resources Research, v. 39, http://onlinelibrary.wiley.com/doi/10.1029/2003WR002086/full (accessed January 2017).

Bowen, G.J., and Wilkinson, B., 2002, Spatial distribution of δ18O in meteoric precipitation: Geology, v. 30, p. 315–318.

Brencher, G., Handwerger, A.L., and Munroe, J.S., 2021, InSAR-based characterization of rock glacier movement in the Uinta Mountains, Utah, USA: The Cryosphere, v. 15, p. 4823–4844.

Brighenti, S., Hotaling, S., Finn, D.S., Fountain, A.G., Hayashi, M., Herbst, D., Saros, J.E., Tronstad, L.M., and Millar, C.I., 2021, Rock glaciers and related cold rocky landforms: Overlooked climate refugia for mountain biodiversity: Global Change Biology, v. 27, p. 1504–1517.

Buchli, T., Kos, A., Limpach, P., Merz, K., Zhou, X., and Springman, S.M., 2018, Kinematic investigations on the Furggwanghorn rock glacier, Switzerland: Permafrost and Periglacial Processes, v. 29, p. 3–20.

Catalan, J., Ninot, J.M., and Aniz, M.M., 2017, High mountain conservation in a changing world: Springer Nature.

Chakraborty, A., 2021, Mountains as vulnerable places: a global synthesis of changing mountain systems in the Anthropocene: GeoJournal, v. 86, p. 585–604.

Craig, H., 1961, Isotopic variations in meteoric waters: Science, v. 133, p. 1702–1703.

Dansgaard, W., 1964, Stable isotopes in precipitation: Tellus, v. 16, p. 436–468.

507   Dehler, C.M., Porter, S.M., De Grey, L.D., Sprinkel, D.A., and Brehm, A., 2007, The Neoproterozoic Uinta
508   Mountain Group revisited; a synthesis of recent work on the Red Pine Shale and related undivided clastic
509   strata, northeastern Utah, U. S. A (P. K. Link & R. S. Lewis, Eds.): Special Publication - Society for
510   Sedimentary Geology, v. 86, p. 151–166.

511   Dietermann, N., and Weiler, M., 2013, Spatial distribution of stable water isotopes in alpine snow cover: Hydrology
512   and Earth System Sciences, v. 17, p. 2657–2668.

513   Earman, S., Campbell, A.R., Phillips, F.M., and Newman, B.D., 2006, Isotopic exchange between snow and
514   atmospheric water vapor: Estimation of the snowmelt component of groundwater recharge in the
515   southwestern United States: Journal of Geophysical Research: Atmospheres, v. 111.

516   Egan, P.A., and Price, M.F., 2017, Mountain ecosystem services and climate change: A global overview of potential
517   threats and strategies for adaptation:

518   von Freyberg, J., Knapp, J.L.A., Rücker, A., Studer, B., and Kirchner, J.W., 2020, Technical note: Evaluation of a
519   low-cost evaporation protection method for portable water samplers: Hydrology and Earth System
520   Sciences, v. 24, p. 5821–5834, doi:10.5194/hess-24-5821-2020.

521   Geiger, S.T., Daniels, J.M., Miller, S.N., and Nicholas, J.W., 2014, Influence of rock glaciers on stream hydrology
522   in the La Sal Mountains, Utah: Arctic, Antarctic, and Alpine Research, v. 46, p. 645–658.

523   Giardino, J.R., Shroder, J.F., and Vitek, J.D., 1987, Rock glaciers: Allen & Unwin London.

524   Giardino, J.R., and Vitek, J.D., 1988, The significance of rock glaciers in the glacial-periglacial landscape
525   continuum: Journal of Quaternary Science, v. 3, p. 97–103, doi:10.1002/jqs.3390030111.

526   Gröning, M., Lutz, H.O., Roller-Lutz, Z., Kralik, M., Gourcy, L., and Pöltenstein, L., 2012, A simple rain collector
527   preventing water re-evaporation dedicated for δ18O and δ2H analysis of cumulative precipitation samples:
528   Journal of Hydrology, v. 448, p. 195–200.

529   Halla, C., Blöthe, J.H., Tapia Baldis, C., Trombotto Liaudat, D., Hilbich, C., Hauck, C., and Schrott, L., 2021, Ice
530   content and interannual water storage changes of an active rock glacier in the dry Andes of Argentina: The
531   Cryosphere, v. 15, p. 1187–1213.

532   Hansen, W.R., 1986, Neogene tectonics and geomorphology of the eastern Uinta Mountains in Utah, Colorado, and
533   Wyoming: United States Geological Survey, Professional Paper, v. 75.

534   Harrington, J.S., Mozil, A., Hayashi, M., and Bentley, L.R., 2018, Groundwater flow and storage processes in an
535   inactive rock glacier: Hydrological Processes, v. 32, p. 3070–3088.

536   Huss, M., Bookhagen, B., Huggel, C., Jacobsen, D., Bradley, R.S., Clague, J.J., Vuille, M., Buytaert, W., Cayan,
537   D.R., and Greenwood, G., 2017, Toward mountains without permanent snow and ice: Earth's Future, v. 5,
538   p. 418–435.

539   Janke, J.R., Ng, S., and Bellisario, A., 2017, An inventory and estimate of water stored in firn fields, glaciers,
540   debris-covered glaciers, and rock glaciers in the Aconcagua River Basin, Chile: Geomorphology, v. 296, p.
541   142–152.

542   Johnson, G., Chang, H., and Fountain, A., 2021, Active rock glaciers of the contiguous United States: geographic
543   information system inventory and spatial distribution patterns: Earth System Science Data, v. 13, p. 3979–
544   3994, doi:10.5194/essd-13-3979-2021.

545 Jones, D.B., Harrison, S., Anderson, K., Selley, H.L., Wood, J.L., and Betts, R.A., 2018, The distribution and
546   hydrological significance of rock glaciers in the Nepalese Himalaya: Global and Planetary Change, v. 160,
547   p. 123–142.

548 Jones, D.B., Harrison, S., Anderson, K., and Whalley, W.B., 2019, Rock glaciers and mountain hydrology: A
549   review: Earth-Science Reviews, v. 193, p. 66–90, doi:10.1016/j.earscirev.2019.04.001.

550 Kenner, R., Phillips, M., Limpach, P., Beutel, J., and Hiller, M., 2018, Monitoring mass movements using
551   georeferenced time-lapse photography: Ritigraben rock glacier, western Swiss Alps: Cold Regions Science
552   and Technology, v. 145, p. 127–134.

553 Konrad, S.K., Humphrey, N.F., Steig, E.J., Clark, D.H., Potter, N., and Pfeffer, W.T., 1999, Rock glacier dynamics
554   and paleoclimatic implications: Geology, v. 27, p. 1131–1134.

555 Krainer, K. et al., 2015, A 10,300-year-old permafrost core from the active rock glacier Lazaun, southern Ötztal
556   Alps (South Tyrol, northern Italy): Quaternary Research, v. 83, p. 324–335,
557   doi:10.1016/j.yqres.2014.12.005.

558 Krainer, K., and Mostler, W., 2002, Hydrology of active rock glaciers: examples from the Austrian Alps: Arctic,
559   Antarctic, and Alpine Research, p. 142–149.

560 Krainer, K., Mostler, W., and Spötl, C., 2007, DISCHARGE FROM ACTIVE ROCK GLACIERS, AUSTRIAN
561   ALPS: A STABLE ISOTOPE APPROACH.: Austrian Journal of Earth Sciences, v. 100.

562 Lechler, A.R., and Niemi, N.A., 2011, The influence of snow sublimation on the isotopic composition of spring and
563   surface waters in the southwestern United States: Implications for stable isotope–based paleoaltimetry and
564   hydrologic studies: Geological Society of America Bulletin, p. B30467-1.

565 Lehmann, B., Anderson, R.S., Bodin, X., Cusicanqui, D., Valla, P.G., and Carcaillet, J., 2022, Alpine rock glacier
566   activity over Holocene to modern timescales (western French Alps): Earth Surface Dynamics Discussions,
567   p. 1–40.

568 McDowell, G., Huggel, C., Frey, H., Wang, F.M., Cramer, K., and Ricciardi, V., 2019, Adaptation action and
569   research in glaciated mountain systems: Are they enough to meet the challenge of climate change? Global
570   Environmental Change, v. 54, p. 19–30.

571 Millar, C.I., and Westfall, R.D., 2010, Distribution and climatic relationships of the American pika (Ochotona
572   princeps) in the Sierra Nevada and western Great Basin, USA; periglacial landforms as refugia in warming
573   climates: Arctic, Antarctic, and Alpine Research, v. 42, p. 76–88.

574 Millar, C.I., Westfall, R.D., Evenden, A., Holmquist, J.G., Schmidt-Gengenbach, J., Franklin, R.S., Nachlinger, J.,
575   and Delany, D.L., 2015, Potential climatic refugia in semi-arid, temperate mountains: Plant and arthropod
576   assemblages associated with rock glaciers, talus slopes, and their forefield wetlands, Sierra Nevada,
577   California, USA: Quaternary International, v. 387, p. 106–121, doi:10.1016/j.quaint.2013.11.003.

578 Minder, J.R., Letcher, T.W., and Liu, C., 2018, The character and causes of elevation-dependent warming in high-
579   resolution simulations of Rocky Mountain climate change: Journal of Climate, v. 31, p. 2093–2113.

580 Munroe, J.S., 2018, Distribution, evidence for internal ice, and possible hydrologic significance of rock glaciers in
581   the Uinta Mountains, Utah, USA: Quaternary Research, v. 90, p. 1–16.

582 Munroe, J.S., 2021, First Investigation of Perennial Ice in Winter Wonderland Cave, Uinta Mountains, Utah, USA:
583   The Cryosphere, v. 15, p. 863–881, doi:doi.org/10.5194/tc-15-863-2021.

584 Munroe, J.S., 2006, Investigating the spatial distribution of summit flats in the Uinta Mountains of northeastern
585   Utah, USA: Geomorphology, v. 75, p. 437–449.

586 Munroe, J.S., and Laabs, B.J.C., 2009, Glacial Geologic Map of the Uinta Mountains Area, Utah and Wyoming.:
587   Utah Geological Survey Miscellaneous Publication 09-4DM, scale Map.

588 Østrem, G., and Brugman, M., 1966, Glacier mass balance measurements: Department of Mines and Technical
589   Surveys, Glaciology Section.

590 Palomo, I., 2017, Climate change impacts on ecosystem services in high mountain areas: a literature review:
591   Mountain Research and Development, v. 37, p. 179–187.

592 Petersen, E.I., Levy, J.S., Holt, J.W., and Stuurman, C.M., 2020, New insights into ice accumulation at Galena
593   Creek Rock Glacier from radar imaging of its internal structure: Journal of Glaciology, v. 66, p. 1–10.

594 Rangecroft, S., Harrison, S., and Anderson, K., 2015, Rock Glaciers as Water Stores in the Bolivian Andes: An
595   Assessment of Their Hydrological Importance: Arctic, Antarctic, and Alpine Research, v. 47, p. 89–98,
596   doi:10.1657/AAAR0014-029.

597 Rödder, D., Schmitt, T., Gros, P., Ulrich, W., and Habel, J.C., 2021, Climate change drives mountain butterflies
598   towards the summits: Scientific reports, v. 11, p. 1–12.

599 Rowan, A.V., Quincey, D.J., Gibson, M.J., Glasser, N.F., Westoby, M.J., Irvine-Fynn, T.D., Porter, P.R., and
600   Hambrey, M.J., 2018, The sustainability of water resources in High Mountain Asia in the context of recent
601   and future glacier change: Geological Society, London, Special Publications, v. 462, p. 189–204.

602 Sakai, A., and Fujita, K., 2017, Contrasting glacier responses to recent climate change in high-mountain Asia:
603   Scientific reports, v. 7, p. 1–8.

604 Sears, J., Graff, P., and Holden, G., 1982, Tectonic evolution of lower Proterozoic rocks, Uinta Mountains, Utah and
605   Colorado: Geological Society of America Bulletin, v. 93, p. 990–997.

606 Sommer, C., Malz, P., Seehaus, T.C., Lippl, S., Zemp, M., and Braun, M.H., 2020, Rapid glacier retreat and
607   downwasting throughout the European Alps in the early 21 st century: Nature Communications, v. 11, p. 1–
608   10.

609 Steig, E.J., Fitzpatrick, J.J., Potter, N., and Clark, D.H., 1998, The geochemical record in rock glaciers: Geografiska
610   Annaler: Series A, Physical Geography, v. 80, p. 277–286.

611 Stoffel, M., and Corona, C., 2018, Future winters glimpsed in the Alps: Nature Geoscience, v. 11, p. 458–460.

612 Strozzi, T., Caduff, R., Jones, N., Barboux, C., Delaloye, R., Bodin, X., Kääb, A., Mätzler, E., and Schrott, L., 2020,
613   Monitoring rock glacier kinematics with satellite synthetic aperture radar: Remote Sensing, v. 12, p. 559.

614 Taylor, S., Feng, X., Kirchner, J.W., Osterhuber, R., Klaue, B., and Renshaw, C.E., 2001, Isotopic evolution of a
615   seasonal snowpack and its melt: Water Resources Research, v. 37, p. 759–769.

616 Thaler, T., Zischg, A., Keiler, M., and Fuchs, S., 2018, Allocation of risk and benefits—distributional justices in
617   mountain hazard management: Regional environmental change, v. 18, p. 353–365.

618 Unnikrishna, P.V., McDonnell, J.J., and Kendall, C., 2002, Isotope variations in a Sierra Nevada snowpack and their
619   relation to meltwater: Journal of Hydrology, v. 260, p. 38–57.

620 Wagner, T., Brodacz, A., Krainer, K., and Winkler, G., 2020, Active rock glaciers as shallow groundwater
621   reservoirs, Austrian Alps: Grundwasser, v. 25, p. 215–230.

622 Wagner, T., Kainz, S., Helfricht, K., Fischer, A., Avian, M., Krainer, K., and Winkler, G., 2021, Assessment of
623   liquid and solid water storage in rock glaciers versus glacier ice in the Austrian Alps: Science of the Total
624   Environment, v. 800, p. 149593.

625 Wahrhaftig, C., and Cox, A., 1959, Rock glaciers in the Alaska Range: Geological Society of America Bulletin, v.
626   70, p. 383–436.

627 Williams, M.W., Knauf, M., Caine, N., Liu, F., and Verplanck, P.L., 2006, Geochemistry and source waters of rock
628   glacier outflow, Colorado Front Range: Permafrost and Periglacial Processes, v. 17, p. 13–33,
629   doi:10.1002/ppp.535.

630 Williams, M.W., Knauf, M., Cory, R., Caine, N., and Liu, F., 2007, Nitrate content and potential microbial signature
631   of rock glacier outflow, Colorado Front Range: Earth Surface Processes and Landforms, v. 32, p. 1032–
632   1047, doi:10.1002/esp.1455.

633 Xenarios, S., Gafurov, A., Schmidt-Vogt, D., Sehring, J., Manandhar, S., Hergarten, C., Shigaeva, J., and Foggin,
634   M., 2019, Climate change and adaptation of mountain societies in Central Asia: uncertainties, knowledge
635   gaps, and data constraints: Regional Environmental Change, v. 19, p. 1339–1352.

636